Journal of Mathematical Modeling
Vol. 4, No. 1, 2016, pp. 59-78

JMM

Modeling and analysis of a three-component piezoelectric force sensor

Fu Shao*

Department of Mechanical and Industrial Engineering, University of Toronto, Toronto, Canada
Email: fu.shao@mail.utoronto.ca

Abstract. This paper presents a mathematical model for the vibration analysis of a three-component piezoelectric force sensor. The cubic theory of weakly nonlinear electroelasticity is applied to the model for describing the electromechanical coupling effect in the piezoelectric sensing elements which operate in thickness-shear and thickness-stretch vibration modes. Hamilton's principle is used to derive motion and charge equations for the vibration analysis. The model can predict the performance of the force sensor for use in proposed cutting force measurement.

Keywords: piezoelectric, force sensor, nonlinear vibration analysis, weakly nonlinear electroelasticity.
AMS Subject Classification: 34A34, 91E45.

1 Introduction

A three-component piezoelectric force sensor, Figure 1, has been designed to address sensing resolution and frequency bandwidth issues that currently exist in the measurement of cutting forces for meso-milling applications [12]. The designed force sensor comprises of six piezoelectric sensing elements which are distributed into three groups, Figure 1(b), for measuring the three components of the cutting forces, $F_{X,Y,Z}$, respectively. Two groups of sensing elements working in thickness-shear mode are used to measure F_X

*Corresponding author.
Received: 8 November 2015 / Revised: 1 June 2016 / Accepted: 1 June 2016.

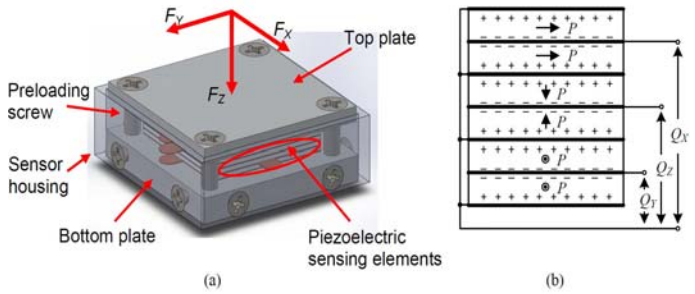

Figure 1: Sensor Model: (a) Components and (b) Output Charges.

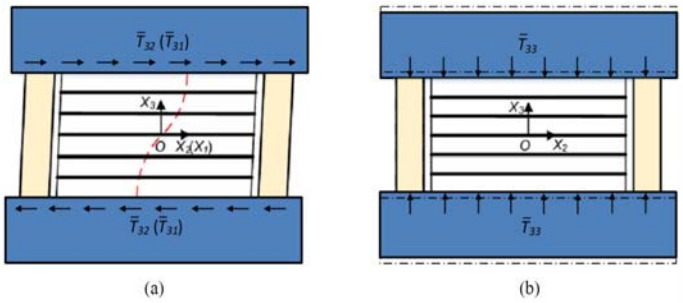

Figure 2: Electromechanical Model for: (a) Thickness-Shear Mode Vibration due to F_X (F_Y), and (b) Thickness-Stretch Mode Vibration due to F_Z.

and F_Y based on output charges Q_X and Q_Y, and one group in thickness-stretch mode is used to measure F_Z based on output charge Q_Z. In Figure 1(b), the thick black lines with $'+'$ and $'-'$ signs represent the positive and negative electrodes of each sensing element, P represents the polarization direction in each sensing element. The force sensor also consists of rigid top and bottom plates which are used to generate homogenous stresses on the piezoelectric sensing elements. Preloading screws are used to exert compression force on the top and bottom plates and the piezoelectric sensing elements in order to provide sufficient friction to avoid slippage between these components. A sensor housing, which is used to protect the piezoelectric sensing elements, is attached to the bottom plate.

Due to the oscillation characteristic of the input cutting forces [12], a vibration analysis model of the sensory system is imperative for analyzing the sensor response, namely the mechanical deformation and output charges, to the input excitation. The sensor response can be used to predict the sensor performance for the measurement: (1) the mechanical deformation and

output charges with respect to the excitation frequency are used to identify the frequency bandwidth, i.e., the linear operating range [2], of the force sensor; (2) the output charges within the frequency bandwidth are used to determine the sensing resolution of the force sensor, i.e., the minimum change in the input signal that the sensor can detect [7]. The development of the vibration analysis model involves the following procedures: (1) mathematical modeling of the vibrations of the sensory system, (2) derivation of the motion and charge equations, (3) analytical solutions with respect to mechanical deformation and output charges, and (4) simulations of sensor response and analysis of sensor performance.

2 Mathematical modeling

The electromechanical model of the overall sensory system under the three-component cutting forces is presented in Figure 2 where the homogeneous stresses, $\bar{T}_{32}$, $\bar{T}_{31}$ and $\bar{T}_{33}$, due to the three components of the cutting forces, $F_{X,Y,Z}$, excite two thickness-shear mode vibrations in X_2 and X_1 axial directions, Figure 2(a), and one thickness-stretch mode vibration in X_3 axial direction, Figure 2(b). For mathematical modeling, the sensor components are divided into deformable components and rigid bodies due to their structural stiffness. The deformable components include the stacked piezoelectric ceramic sensing elements and the parallel preloading screws which deform under the cutting forces, as shown in Figure 2. The rigid body associated with the top surface of the deformable components includes sensor top plate, and the proposed workpiece and fixture that will be attached to the sensor top plate. The rigid body associated with the bottom surface of the deformable components includes sensor bottom plate and sensor housing. For mathematical modeling, the mass of the top rigid body is assumed to be equal to that of the bottom rigid body so that the reference coordinates, $X_{1,2,3}$, can be fixed at the central point of the stacked piezoelectric sensing elements and the symmetry of the sensory system can be used in the modeling.

In order to determine the linear operating range of a piezoelectric device, a nonlinear vibration analysis model is necessary [5, 14]. The nonlinear vibration analysis model is used herein to analyze the nonlinear effect, namely the large mechanical deformation and distorted output charges, of the sensory system with excitation frequency approaching the fundamental natural frequencies of the force sensor. The nonlinear effect is then used to determine the linear operating range of the force sensor where the amplitude of the mechanical deformation and the amplitude of the output

charges are only determined by the amplitude of the input cutting forces and are independent of the excitation frequency. The development of the nonlinear vibration analysis model comprises of using the theory of nonlinear electroelasticity [15,17] for the piezoelectric sensing elements, the three dimensional elasticity theory [9] for the preloading screws, and the kinetic energy equation for the rigid bodies. The theory of nonlinear electroelasticity is pertinent for modeling the nonlinear effect in piezoelectric components due to resonance [16]. Within these theories, the energy functional of the overall sensory system is formulated as:

$$\begin{aligned} I(y_m,\phi) = &\int_{t_0}^{t_1} dt \int_0^{V_0} \left\{ \frac{\rho_0}{2}\dot{y}_m^2 - \rho_0\hat{\psi}\left(\varepsilon_{LM},\mathcal{E}_K\right) - \rho_E\phi \right\} dV \\ &+ \int_{t_0}^{t_1} dt \int_0^{V_1} \left\{ \frac{\rho_1}{2}\dot{y}_m^2 - \rho_1\pi\left(\varepsilon_{LM}\right) \right\} dV \\ &+ \int_{t_0}^{t_1} dt \int_0^{V_2} \frac{\rho_1}{2}\dot{y}_m^2 \mid_{X_3=3h} dV + \int_{t_0}^{t_1} dt \int_0^{V_3} \frac{\rho_1}{2}\dot{y}_m^2 \mid_{X_3=-3h} dV \\ &+ \int_{t_0}^{t_1} dt \int_0^{\bar{S}_T} \bar{T}_{LM} y_m dS - \int_{t_0}^{t_1} dt \int_0^{\bar{S}_D} \bar{\sigma}_E \phi dS, \end{aligned} \tag{1}$$

where ρ_0 and ρ_1 represent the density of the piezoelectric material used for the sensing elements and the density of the steel material used for the rest sensor components. ρ_E represents the reference charge density in the piezoelectric sensing elements. y_m represents the motion of a material point in the sensor components due to the vibrations, $m = 1,2,3$ defining the directions of the motion along the reference coordinates, $X_{1,2,3}$. ϕ is the electric potential in the piezoelectric sensing elements. $\hat{\psi}\left(\varepsilon_{LM},\mathcal{E}_K\right)$ and $\pi\left(\varepsilon_{LM}\right)$ are referred to as energy densities due to the deformation in the stacked piezoelectric sensing elements and the parallel preloading screws. ε_{LM} represents the strain in the deformable sensor components and $\mathcal{E}_K$ represents the electric field in the piezoelectric sensing elements. Indices L, M define the vibration mode of the sensory system and index K defines the electric field direction in the piezoelectric sensing elements. V_0, V_1, V_2 and V_3 represent the volume of the stacked piezoelectric sensing elements, the parallel preloading screws, the top rigid body, and the bottom rigid body. h represents the thickness of each piezoelectric sensing element. $\bar{T}_{LM}$ represents the stresses distributed on the deformable sensor components due to cutting forces $F_{X,Y,Z}$, and S_T represents the area of the top and bottom surfaces of the deformable components where $\bar{T}_{LM}$ is exerted onto. σ_E represents the density of the free charges distributed on the surface S_D of each piezoelectric sensing element due to the electromechanical coupling

effect. For the nonlinear vibration analysis, the strain ε_{LM} is defined for the deformable components as [15]:

$$\varepsilon_{LM} = \frac{1}{2}\left(\frac{\partial y_m}{\partial X_M}\frac{\partial y_m}{\partial X_L} - \delta_{LM}\right), \tag{2}$$

where δ_{LM} is the Kronecker delta. The electric field $\mathcal{E}_K$ in each piezoelectric sensing element is defined as [15]:

$$\mathcal{E}_K = -\frac{\partial \phi}{\partial X_K}. \tag{3}$$

3 Motion and charge equations

Within Hamilton's principle [1], the first variation of (1) with respect to variables y_m and ϕ gives (integration by parts is applied to the quadratic terms in (1) for the first variation as illustrated in the Appendix):

$$\begin{aligned}
\delta I(y_m,\phi) = &-\int_{t_0}^{t_1} dt \int_0^{V_0} \left\{ \rho_0 \ddot{y}_m \delta y_m + \rho_0 \frac{\partial \hat{\psi}\left(\varepsilon_{LM}, \mathcal{E}_K\right)}{\partial \varepsilon_{LM}} \delta \varepsilon_{LM} \right\} dV \\
&-\int_{t_0}^{t_1} dt \int_0^{V_0} \left\{ \rho_0 \frac{\partial \hat{\psi}\left(\varepsilon_{LM}, \mathcal{E}_K\right)}{\partial \mathcal{E}_K} \delta \mathcal{E}_K + \rho_E \delta \phi \right\} dV \\
&-\int_{t_0}^{t_1} dt \int_0^{V_1} \left\{ \rho_1 \ddot{y}_m \delta y_m + \rho_1 \frac{d\pi\left(\varepsilon_{LM}\right)}{d\varepsilon_{LM}} \delta \varepsilon_{LM} \right\} dV \\
&-\int_{t_0}^{t_1} dt \int_0^{V_2} \left(\rho_1 \ddot{y}_m \delta y_m\right) |_{X_3=3h}\, dV \\
&+\int_{t_0}^{t_1} dt \int_0^{V_3} \left(\rho_1 \ddot{y}_m \delta y_m\right) |_{X_3=-3h}\, dV \\
&+\int_{t_0}^{t_1} dt \int_0^{\bar{S}_T} \bar{T}_{LM} \delta y_m dS - \int_{t_0}^{t_1} dt \int_0^{\bar{S}_D} \bar{\sigma}_E \delta \phi dS = 0.
\end{aligned} \tag{4}$$

From (2) and (3), and following the chain rule [10] and the commutativity between the operators [11], the variation of the strain and the variation of the electric field are defined as:

$$\begin{aligned}
\delta \varepsilon_{LM} &= \delta\left\{\frac{1}{2}\left(\frac{\partial y_m}{\partial X_M}\frac{\partial y_m}{\partial X_L} - \delta_{LM}\right)\right\} \\
&= \frac{1}{2}\left\{\frac{\delta\left(\partial y_m\right)}{\partial X_L}\frac{\partial y_m}{\partial X_M} + \frac{\partial y_m}{\partial X_L}\frac{\delta\left(\partial y_m\right)}{\partial X_M}\right\} = \frac{\partial y_m}{\partial X_M}\frac{\partial}{\partial X_L}\delta y_m,
\end{aligned} \tag{5}$$

$$\delta\mathcal{E}_K = \delta\left(-\frac{\partial\phi}{\partial X_K}\right) = -\frac{\partial}{\partial X_K}\delta\phi. \tag{6}$$

Equation (4) is then rewritten as:

$$\begin{aligned}
&\delta I(y_m,\phi)\\
&= -\int_{t_0}^{t_1} dt \int_0^{V_0} \left\{ \rho_0 \ddot{y}_m \delta y + \frac{\partial y_m}{\partial X_M}\rho_0 \frac{\partial \hat{\psi}\left(\varepsilon_{LM},\mathcal{E}_K\right)}{\partial \varepsilon_{LM}} \frac{\partial}{\partial X_L}\delta y_m \right\} dV\\
&\quad + \int_{t_0}^{t_1} dt \int_0^{V_0} \left\{ \rho_0 \frac{\partial \hat{\psi}\left(\varepsilon_{LM},\mathcal{E}_K\right)}{\partial \mathcal{E}_K} \frac{\partial}{X_K}\delta\phi - \rho_E \delta\phi \right\} dV\\
&\quad - \int_{t_0}^{t_1} dt \int_0^{V_1} \left\{ \rho_1 \ddot{y}_m \delta y + \frac{\partial y_m}{\partial X_M}\rho_1 \frac{d\pi\left(\varepsilon_{LM}\right)}{d\varepsilon_{LM}} \frac{\partial}{\partial X_L}\delta y_m \right\} dV\\
&\quad - \int_{t_0}^{t_1} dt \int_0^{V_2} \left(\rho_1 \ddot{y}_m \delta y\right)|_{X_3=3h}\, dV\\
&\quad + \int_{t_0}^{t_1} dt \int_0^{V_3} \left(\rho_1 \ddot{y}_m \delta y\right)|_{X_3=-3h}\, dV\\
&\quad + \int_{t_0}^{t_1} dt \int_0^{\bar{S}_T} \bar{T}_{LM}\delta y_M dS - \int_{t_0}^{t_1} dt \int_0^{\bar{S}_D} \bar{\sigma}_E \delta\phi dS = 0,
\end{aligned} \tag{7}$$

where $\frac{\partial y_m}{\partial X_M}\rho_0\frac{\partial\hat{\psi}(\varepsilon_{LM},\mathcal{E}_K)}{\partial\varepsilon_{LM}}$ and $\rho_0\frac{\partial\hat{\psi}(\varepsilon_{LM},\mathcal{E}_K)}{\partial\mathcal{E}_K}$ are defined as two-point total stress tensor, $\hat{K}_{Lm}$, and reference electric displacement, D_K, for the piezoelectric electric sensing elements as [15]:

$$\hat{K}_{Lm} = \frac{\partial y_m}{\partial X_M}\rho_0\frac{\partial\hat{\psi}\left(\varepsilon_{LM},\mathcal{E}_K\right)}{\partial\varepsilon_{LM}}, \tag{8}$$

$$D_K = -\rho_0\frac{\partial\hat{\psi}\left(\varepsilon_{LM},\mathcal{E}_K\right)}{\partial\mathcal{E}_K}. \tag{9}$$

Similarly, $\frac{\partial y_m}{\partial X_M}\rho_1\frac{d\pi(\varepsilon_{LM})}{d\varepsilon_{LM}}$ is defined as two-point total stress tensor, K_{Lm}, for the preloading screws as:

$$K_{Lm} = \frac{\partial y_m}{\partial X_M}\rho_1\frac{d\pi\left(\varepsilon_{LM}\right)}{d\varepsilon_{LM}}. \tag{10}$$

Substitute (8) to (10) into (7) and integrate the first and second integrals in (7) by parts, (7) is rewritten as:

$$
\begin{aligned}
&\delta I(y_m,\phi)\\
&=-\int_{t_0}^{t_1}dt\int_0^{V_0}\{\rho_0\ddot{y}_m\delta y+\rho_E\delta\phi\}\,dV\\
&\quad-\int_{t_0}^{t_1}dt\int_0^{S_T}dS\left\{\hat{K}_{Lm}\delta y_m|_0^{X_L}-\int_0^{X_L}\hat{K}_{Lm,L}\delta y_m dX_L\right\}\\
&\quad-\int_{t_0}^{t_1}dt\int_0^{S_D}dS\left\{D_K\delta\phi|_0^{X_K}-\int_0^{X_K}D_{K,K}\delta\phi dX_K\right\}\\
&\quad+\int_{t_0}^{t_1}dt\frac{S_T-S_D}{S_D}\int_0^{V_0}\{-\rho_1\ddot{y}_m\delta y\}\,dV\\
&\quad-\int_{t_0}^{t_1}dt\frac{S_T-S_D}{S_D}\int_0^{S_T}dS\left\{K_{Lm}\delta y_m|_0^{X_L}-\int_0^{X_L}K_{Lm,L}\delta y_m dX_L\right\}\\
&\quad-\int_{t_0}^{t_1}dt\int_0^{V_2}(\rho_1\ddot{y}_m\delta y)\,|_{X_3=3h}\,dV+\int_{t_0}^{t_1}dt\int_0^{V_3}(\rho_1\ddot{y}_m\delta y)\,|_{X_3=-3h}\,dV\\
&\quad+\int_{t_0}^{t_1}dt\int_0^{\bar{S}_T}\bar{T}_{LM}\delta y_M dS-\int_{t_0}^{t_1}dt\int_0^{\bar{S}_D}\bar{\sigma}_E\delta\phi dS\\
&=\int_{t_0}^{t_1}dt\int_0^{V_0}\left\{-\rho_0\ddot{y}_m-\frac{S_T-S_D}{S_D}\rho_1\ddot{y}_m\right\}\delta y_m dV\\
&\quad+\int_{t_0}^{t_1}dt\int_0^{V_0}\left\{\hat{K}_{Lm,L}+\frac{S_T-S_D}{S_D}K_{Lm,L}\right\}\delta y_m dV\\
&\quad+\int_{t_0}^{t_1}dt\int_0^{V_0}\{\mathcal{D}_{K,K}-\rho_E\}\,\delta\phi dV+\int_{t_0}^{t_1}dt\int_0^{\bar{S}_T}\bar{T}_{LM}\delta y_M dS\\
&\quad-\int_{t_0}^{t_1}dt\int_0^{\bar{S}_T}\left(\hat{K}_{Lm}+\frac{S_T-S_D}{S_D}K_{Lm}\right)N_L\delta y_M dS\\
&\quad-\int_{t_0}^{t_1}dt\int_0^{V_2}(\rho_1\ddot{y}_m\delta y)\,|_{X_3=3h}\,dV+\int_{t_0}^{t_1}dt\int_0^{V_3}(\rho_1\ddot{y}_m\delta y)\,|_{X_3=-3h}\,dV\\
&\quad-\int_{t_0}^{t_1}dt\int_0^{\bar{S}_D}\{\mathcal{D}_K N_K+\bar{\sigma}_E\}\,\delta\phi dS=0,
\end{aligned}
\tag{11}
$$

where N_L and N_K represent the unit normal of the stress and electric boundary surfaces, respectively. Separate the terms in (11) with respect to δy_m and $\delta\phi$, the motion and charge equations of the sensory system are

formulated as:

$$\hat{K}_{Lm,L} + \frac{S_T - S_D}{S_D} K_{Lm,L} = \left(\rho_0 + \frac{S_T - S_D}{S_D}\rho_1\right) \ddot{y}_m, \tag{12}$$

$$\mathcal{D}_{K,K} = \rho_E, \tag{13}$$

and the stress and electric boundary conditions are formulated as:

$$\begin{aligned} &\int_0^{S_T} \left(\hat{K}_{Lm} + \frac{S_T - S_D}{S_D} K_{Lm}\right) N_L dS + \int_0^{V_2} (\rho_1 \ddot{y}_m) \mid_{X_3=3h} dV \\ &- \int_0^{V_3} (\rho_1 \ddot{y}_m) \mid_{X_3=-3h} dV = \int_0^{S_T} \bar{T}_{LM} dS, \end{aligned} \tag{14}$$

$$\mathcal{D}_K N_K = -\bar{\sigma}_E. \tag{15}$$

The displacement vector for the motion of a material point can be defined as [15]:

$$\mathbf{u} = \mathbf{y} - \mathbf{X}, \tag{16}$$

where $\mathbf{u}$ represents the displacement vector of a material point, $\mathbf{y}$ represents the present position vector of the material point, and $\mathbf{X}$ is constant which represents the original position vector of the material point. The differential of (16) over time gives:

$$\dot{\mathbf{u}} = \dot{\mathbf{y}}, \tag{17}$$

$$\ddot{\mathbf{u}} = \ddot{\mathbf{y}}. \tag{18}$$

From (18), (12) is rewritten with displacement term as:

$$\hat{K}_{Lm,L} + \frac{S_T - S_D}{S_D} K_{Lm,L} = \left(\rho_0 + \frac{S_T - S_D}{S_D}\rho_1\right) \ddot{u}_m. \tag{19}$$

Relating $\hat{K}_{Lm}$, K_{Lm}, and u_m to the reference coordinates by denoting [17]:

$$\hat{K}_{LM} = \hat{K}_{Lm}\delta_{mM}, \tag{20}$$

$$K_{LM} = K_{Lm}\delta_{mM}, \tag{21}$$

$$u_M = u_m\delta_{mM}, \tag{22}$$

the motion equation presented in (19) is then rewritten as:

$$\hat{K}_{LM,L} + \frac{S_T - S_D}{S_D} K_{LM,L} = \left(\rho_0 + \frac{S_T - S_D}{S_D}\rho_1\right) \ddot{u}_M, \tag{23}$$

and the stress boundary condition presented in (14) is rewritten as:

$$\begin{aligned}&\int_0^{S_T}\left(\hat{K}_{LM}+\frac{S_T-S_D}{S_D}K_{LM}\right)N_L dS+\int_0^{V_2}\left(\rho_1\ddot{u}_M\right)|_{X_3=3h}\,dV\\&-\int_0^{V_3}\left(\rho_1\ddot{u}_M\right)|_{X_3=-3h}\,dV=\int_0^{S_T}\bar{T}_{LM}dS.\end{aligned}\tag{24}$$

A charge mode amplifier [6] will be used to amplify the sensor output charge signals for subsequent data acquisition and processing. Since the charge mode amplifier maintains a weak electric field in each sensing element, the cubic theory of weakly nonlinear electroelasticity [17] is sufficient to model the electromechanical coupling effect in the piezoelectric sensing elements. Within the cubic theory of weakly nonlinear electroelasticity, the energy density due to the deformation of the piezoelectric sensing elements is defined as [17]:

$$\begin{aligned}\rho_0\hat{\psi}\left(\varepsilon_{LM},\mathcal{E}_K\right)=&\frac{1}{2}c_{ABCD}\varepsilon_{AB}\varepsilon_{CD}+\frac{1}{6}c_{ABCDEF}\varepsilon_{AB}\varepsilon_{CD}\varepsilon_{EF}\\&+\frac{1}{24}c_{ABCDEFGH}\varepsilon_{AB}\varepsilon_{CD}\varepsilon_{EF}\varepsilon_{GH}-e_{ABC}\mathcal{E}_A\varepsilon_{BC}\\&-\frac{1}{2}\chi_{AB}\mathcal{E}_A\mathcal{E}_B.\end{aligned}\tag{25}$$

With the partial differential of (25) and keeping up to the cubic terms of displacement, the two-point total stress tensor $\hat{K}_{LM}$ in piezoelectric sensing elements is defined as [17]:

$$\begin{aligned}\hat{K}_{LM}=&\frac{\partial y_m}{\partial X_M}\rho_0\frac{\partial\hat{\psi}\left(\varepsilon_{LM},\mathcal{E}_K\right)}{\partial\varepsilon_{LM}}\delta_{iM}\\=&c_{LMRS}\frac{\partial u_R}{\partial X_S}+e_{KLM}\frac{\partial\phi}{\partial X_K}+\hat{c}_{LMRSKN}\frac{\partial u_R}{\partial X_S}\frac{\partial u_K}{\partial X_N}\\&+\hat{c}_{LMRSKNIJ}\frac{\partial u_R}{\partial X_S}\frac{\partial u_K}{\partial X_N}\frac{\partial u_I}{\partial X_J},\end{aligned}\tag{26}$$

and the reference electric displacement $\mathcal{D}_K$ in piezoelectric sensing elements is defined as [17]:

$$\begin{aligned}D_K=&-\rho_0\frac{\partial\hat{\psi}\left(\varepsilon_{LM},\mathcal{E}_K\right)}{\partial\mathcal{E}_K}\\=&e_{KRS}\frac{\partial u_R}{\partial X_S}-\xi_{KL}\frac{\partial\phi}{\partial X_L}.\end{aligned}\tag{27}$$

Similarly, within the theory of weakly nonlinear elasticity [8], the energy density due to the deformation in the parallel preloading screws is defined

as:

$$\begin{aligned}\rho_1\pi\left(\varepsilon_{LM}\right) = &\frac{1}{2}c_{ABCD}\varepsilon_{AB}\varepsilon_{CD} + \frac{1}{6}c_{ABCDEF}\varepsilon_{AB}\varepsilon_{CD}\varepsilon_{EF} \\ &+ \frac{1}{24}c_{ABCDEFGH}\varepsilon_{AB}\varepsilon_{CD}\varepsilon_{EF}\varepsilon_{GH}.\end{aligned} \tag{28}$$

With the differential of (28) and keeping up to the cubic terms of displacements, the two-point total stress tensor K_{LM} in preloading screws is defined as:

$$\begin{aligned}K_{LM} &= \frac{\partial y_m}{\partial X_M}\rho_1\frac{d\pi\left(\varepsilon_{LM}\right)}{d\varepsilon_{LM}}\delta_{iM} \\ &= c_{LMRS}\frac{\partial u_R}{\partial X_S} + \hat{c}_{LMRSKN}\frac{\partial u_R}{\partial X_S}\frac{\partial u_K}{\partial X_N} \\ &+ \hat{c}_{LMRSKNIJ}\frac{\partial u_R}{\partial X_S}\frac{\partial u_K}{\partial X_N}\frac{\partial u_I}{\partial X_J},\end{aligned} \tag{29}$$

where $\hat{c}_{LMRSKN}$ and $\hat{c}_{LMRSKNIJ}$ are given by [17]:

$$\hat{c}_{LMRSKN} = \frac{1}{2}\left(c_{LMRSKN} + c_{LMNS}\delta_{KR} + c_{LNRS}\delta_{KM}\right), \tag{30}$$

$$\begin{aligned}\hat{c}_{LMRSKNIJ} = &\frac{1}{6}c_{LMRSKNIJ} \\ &+ \frac{1}{2}\left(c_{LMKNSJ}\delta_{RI} + c_{LNSJ}\delta_{MK}\delta_{RI} + c_{LNRSIJ}\delta_{MK}\right),\end{aligned} \tag{31}$$

c_{LMRS}, c_{LMNS}, c_{LNRS} and c_{LNSJ} represent the second order elastic constants, c_{LMRSKN}, c_{LMKNSJ} and c_{LNRSIJ} represent the third order elastic constants, $c_{LMRSKNIJ}$ represents the fourth order elastic constant. δ_{iM}, δ_{KR}, δ_{KM}, δ_{RI} and δ_{MK} are the Kronecker deltas. e_{KLM} and e_{KRS} represent the piezoelectric stress constants of the sensing element material. ξ_{KL} represents the dielectric coefficient of the sensing element material. χ_{AB} is the electric susceptibility.

4 Analytical solutions

The vibration analysis model is solved for the mechanical deformation of the sensory system and the output charges of each sensing element group due to the input cutting forces. Thin plate structure is used herein for the piezoelectric sensing elements so that edge effect can be ignored [14, 16]. Namely, the mechanical deformation, represented by u_M, and the electric potential in the sensing element are independent of the spatial variables X_1 and X_2 [14].

4.1 Mechanical deformation

Due to the top and bottom rigid bodies, the mechanical deformation of the force sensor are equal to the mechanical deformation of the deformable sensor components. The displacement u_M in the deformable sensor components is defined as [14]:

$$u_M\left(X_3,t\right)\cong u\left(t\right)\sin\frac{\pi}{6h}X_3, \tag{32}$$

the mechanical deformation of the force sensor is determined by the difference of the displacement between the top and bottom surfaces of the deformable sensor components as:

$$u_M\left(3h,t\right)-u_M\left(-3h,t\right)=2u\left(t\right), \tag{33}$$

where $M=1,2,3$ corresponding to the mechanical deformation in $X_{1,2,3}$ directions.

4.2 Output charges

The output charges of each sensing element group are determined by solving (13) for the electric displacement $\mathcal{D}_K$. From (13) and (27), the partial differential of ϕ gives:

$$\frac{\partial^2\phi}{\partial X_L^2}=\frac{e_{KLM}}{\xi_{KL}}\frac{\partial^2 u_M}{\partial X_L^2}, \tag{34}$$

where $L=3$ corresponding to the spatial variable X_3 and $K=3$ corresponding to the electric field which is also defined in X_3 direction.

Integration of (34) results in:

$$\frac{\partial\phi}{\partial X_L}=\frac{e_{KLM}}{\xi_{KL}}\frac{\partial u_M}{\partial X_L}+C_1\left(t\right), \tag{35}$$

$$\phi=\frac{e_{KLM}}{\xi_{KL}}u_M+C_1\left(t\right)X_L+C_2\left(t\right). \tag{36}$$

Substitute (35) into (27) and isolate (27) for $C_1\left(t\right)$:

$$\mathcal{D}_K=e_{KLM}\frac{\partial u_M}{\partial X_M}-\xi_{KL}\left(\frac{e_{KLM}}{\xi_{KL}}\frac{\partial u_M}{\partial X_L}+C_1\left(t\right)\right)=-\xi_{KL}C_1\left(t\right). \tag{37}$$

Using the electric boundary condition presented in (15) and the expression of $\mathcal{D}_K$ presented in (37), the output charges for each sensing element group are determined by $C_1\left(t\right)$ as [5]:

$$Q=2\int_0^{S_D}\bar{\sigma}_E dS=2\int_0^{S_D}\left(-D_K\right)dS=2S_D\xi_{KL}C_1\left(t\right). \tag{38}$$

4.3 Solution method

The vibration model presented in (23) is solved by the method of separating the spatial variable X_3 and time t with the use of (32) for the expression of displacement u_M and (24) for the expression of the stress boundary condition. Since the linear operating range is approximated as 1/3 of the minimum fundamental natural frequency [4], the fundamental natural frequencies of the three dimensional vibrations are of interest herein for the analysis. Within Hamilotn's principle, the following variational equation is used to solve the vibration model:

$$\int_{-3h}^{3h} \left\{ \hat{K}_{LM,L} + \frac{S_T - S_D}{S_D} K_{LM,L} - \left(\rho_0 + \frac{S_T - S_D}{S_D} \rho_1 \right) \ddot{u}_M \right\} \delta u_M dX_L = 0. \tag{39}$$

Integrating (39) by parts and utilizing (24) for the stress boundary condition, we obtain:

$$\begin{aligned} &\left\{ \hat{K}_{LM} + \frac{S_T - S_D}{S_D} K_{LM} \right\} \sin\left(\frac{\pi}{6h} X_L\right) |_{-3h}^{3h} \\ &+ \left\{ \frac{6h}{\pi} \left(\rho_0 + \frac{S_T - S_D}{S_D} \rho_1 \right) \ddot{u}(t) \cos\left(\frac{\pi}{6h} X_L\right) \right\} \sin\left(\frac{\pi}{6h} X_L\right) |_{-3h}^{3h} \\ &- \int_{-3h}^{3h} \left\{ \hat{K}_{LM} + \frac{S_T - S_D}{S_D} K_{LM} \right\} \cos\left(\frac{\pi}{6h} X_L\right) d\left(\frac{\pi}{6h} X_L\right) \\ &- \int_{-3h}^{3h} \left\{ \frac{6h}{\pi} \left(\rho_0 + \frac{S_T - S_D}{S_D} \rho_1 \right) \ddot{u}(t) \cos\left(\frac{\pi}{6h} X_L\right) \right\} \cos\left(\frac{\pi}{6h} X_L\right) d\left(\frac{\pi}{6h} X_L\right) \\ &= 0, \end{aligned} \tag{40}$$

where

$$\begin{aligned} &\left\{ \hat{K}_{LM} + \frac{S_T - S_D}{S_D} K_{LM} \right\} \sin\left(\frac{\pi}{6h} X_L\right) |_{-3h}^{3h} \\ &\quad + \left\{ \frac{6h}{\pi} \left(\rho_0 + \frac{S_T - S_D}{S_D} \rho_1 \right) \ddot{u}(t) \cos\left(\frac{\pi}{6h} X_L\right) \right\} \sin\left(\frac{\pi}{6h} X_L\right) |_{-3h}^{3h} \\ &= 2 \left\{ \hat{K}_{LM} + \frac{S_T - S_D}{S_D} K_{LM} \right\} \\ &= 2\bar{T}_{LM} - \frac{2}{S_T} \int_0^{V_2} \left(\rho_1 \ddot{u}(t) \sin\left(\frac{\pi}{6h} X_L\right) \right) |_{X_3 = 3h} \, dV \\ &\quad + \frac{2}{S_T} \int_0^{V_3} \left(\rho_1 \ddot{u}(t) \sin\left(\frac{\pi}{6h} X_L\right) \right) |_{X_3 = -3h} \, dV \\ &= 2 \left\{ \bar{T}_{LM} - \frac{\rho_1}{S_T} (V_2 + V_3) \ddot{u}(t) \right\}, \end{aligned} \tag{41}$$

$$\begin{aligned}
&\int_{-3h}^{3h}\left\{\hat{K}_{LM}+\frac{S_T-S_D}{S_D}K_{LM}\right\}\cos\left(\frac{\pi}{6h}X_L\right)d\left(\frac{\pi}{6h}X_L\right)\\
&+\int_{-3h}^{3h}\left\{\frac{6h}{\pi}\left(\rho_0+\frac{S_T-S_D}{S_D}\rho_1\right)\ddot{u}\left(t\right)\cos\left(\frac{\pi}{6h}X_L\right)\right\}\cos\left(\frac{\pi}{6h}X_L\right)d\left(\frac{\pi}{6h}X_L\right)\\
&=\frac{1}{12h}\left\{\left(c^0_{LMML}+\frac{S_T-S_D}{S_D}c^1_{LMML}\right)\pi^2+\frac{e^2_{KLM}\pi}{\xi KK}\alpha\right\}u\left(t\right)+2e_{KLM}C_1\left(t\right)\\
&+\frac{\left(\hat{c}^0_{LMMLML}+\dfrac{S_T-S_D}{S_D}\hat{c}^1_{LMMLML}\right)\pi^2}{27h^2}u^2\left(t\right)\\
&+\frac{\left(\hat{c}^0_{LMMLMLML}+\dfrac{S_T-S_D}{S_D}\hat{c}^1_{LMMLMLML}\right)\pi^4}{576h^3}u^3\left(t\right),
\end{aligned}\tag{42}$$

where $\alpha=\frac{\pi}{3}+\frac{\sqrt{3}}{2}$ for thickness-stretch mode vibration and $\alpha=\frac{\pi}{3}-\frac{\sqrt{3}}{4}$ for thickness-shear mode vibrations. Combining (41) and (42) into (40) and normalizing the resultant, an ODE is obtained to describe the vibration motions:

$$\ddot{u}\left(t\right)+\omega_1^2u\left(t\right)+\gamma u^2\left(t\right)+\eta u^3\left(t\right)+\lambda C_1\left(t\right)=\frac{2\bar{T}_{LM}}{\alpha}\sin\left(\omega t\right),\tag{43}$$

where the fundamental natural frequency ω_1 is defined as:

$$\omega_1=\frac{1}{6h}\sqrt{\frac{\left(\hat{c}^0_{LMML}+\dfrac{S_T-S_D}{S_D}\hat{c}^1_{LMML}\right)\pi^2+\dfrac{e^2_{KLM}\pi}{\xi_{KK}}\alpha}{12h\mu}},\tag{44}$$

and the other parameters are $\gamma=\dfrac{\left(\hat{c}^0_{LMMLML}+\dfrac{S_T-S_D}{S_D}\hat{c}^1_{LMMLML}\right)\pi^2}{27h^2\alpha}$,
$\eta=\dfrac{\left(\hat{c}^0_{LMMLMLML}+\dfrac{S_T-S_D}{S_D}\hat{c}^1_{LMMLMLML}\right)\pi^4}{576h^3\alpha}$, $\lambda=\dfrac{e_{KLM}}{2\alpha}$,
$\mu=3h\left(\rho_0+\dfrac{S_T-S_D}{S_D}\rho_1\right)+\frac{\rho_1}{S_T}\left(V_2+V_3\right)$. $\bar{T}_{LM}$ represents the amplitude of the stresses due to the three components of the cutting forces, $F_{X,Y,Z}$. ω represents the oscillation frequency of the input cutting forces.

The electric boundary condition due to the common ground connection, Figure 1(b), is defined as:

$$\phi\left(X_3+h,t\right)=\phi\left(X_3-h,t\right),\tag{45}$$

where $X_3 = +2h, 0, 2h$ for the top, middle, and bottom sensing element groups, respectively. Using the definition of ϕ presented in (36), the following equation is formulated which forms a function set with (43) for solving for $u(t)$ and $C_1(t)$:

$$\frac{e_{KLM}}{\nu \xi_{KL}} u(t) + 2hC_1(t) = 0, \tag{46}$$

where $\nu = 1$ for thickness-stretch mode vibration and $\nu = 2$ for thickness-shear mode vibrations.

5 Simulations and analysis

The function set presented in (43) and (46) was solved in MATLAB® for the sensor response, namely the mechanical deformation and the output charges which are determined by $u(t)$ and $C_1(t)$, respectively. Simulations of sensor response were performed with sensor component dimensions and material parameters presented in Tables 1 to 3. Since the mechanical deformation and the output charges possess the same oscillation characteristic with the input cutting forces, the amplitude of the mechanical deformation and the amplitude of the output charges can be used to analyze the sensor performance, namely, frequency bandwidth and sensing resolution. The requirements on the sensor design are that the force sensor can provide a sensing resolution of within 10 mN and a frequency bandwidth of up to 8.3 kHz [12].

Table 1: Sensor Components' Material and Dimensions [12].

Sensor Components	Material	Dimensions (mm^3)	Quantity
Sensing elements	BM800	$16.00 \times 16.00 \times 0.50$	6
Top plate	A2 (304)	$22.00 \times 22.00 \times 1.80$	1
Bottom plate	A2 (304)	$22.40 \times 22.40 \times 3.30$	1
Sensor housing	A2 (304)	$22.40 \times 22.40 \times 0.50$	1
Preloading screws	A2 (304)	M2	4

Note: The size of sensor housing is in the format of inner side length × inner side width × thickness.

5.1 Fundamental natural frequencies

Figure 3 presents the fundamental natural frequencies of the three mode vibrations of the sensory system with respect to different sensing element

Table 2: Parameters of BM800 Used in the Simulations [13].

		Thickness-Shear Mode Vibration due to F_X	Thickness-Shear Mode Vibration due to F_Y	Thickness-Stretch Mode Vibration due to F_Z
Mass density (kg/m^3)			$\rho_0 = 7600$	
Dielectric coefficient $(10^{-12}F/m)$			$\xi_{33} = 8854$	
Elastic constants $(10^{10}N/m^2)$		$c^0_{44} = 3.33$ $\hat{c}^0_{444} = 0$ $\hat{c}^0_{4444} = 7.32$	$c^0_{55} = 3.33$ $\hat{c}^0_{555} = 0$ $\hat{c}^0_{5555} = 7.32$	$c^0_{33} = 14.63$ $\hat{c}^0_{333} = 14.63$ $\hat{c}^0_{3333} = 7.32$
Piezo-stress constants (C/m^2)	top middel bottom	$e^0_{34} = 9.50$ $e^0_{34} = 0$ $e^0_{34} = 0$	$e^0_{35} = 0$ $e^0_{35} = 0$ $e^0_{35} = 9.50$	$e^0_{33} = 0$ $e^0_{33} = 21.21$ $e^0_{33} = 0$

Note: Top, middle, and bottom represent the top, middle, and bottom groups, respectively, of the stacked piezoelectric sensing elements.

thicknesses. For the proposed 0.5 mm sensing element thickness, the fundamental natural frequencies are identified to be 37.0 kHz for thickness-shear mode vibrations and 76.2 kHz for the thickness-stretch mode vibration.

5.2 Frequency bandwidth

The amplitude of the mechanical deformation and the amplitude of the output charges are presented in Figure 4 and Figure 5, respectively, with respect to the excitation frequency approaching the fundamental natural frequencies. As can be seen from Figure 4, the relationship between the mechanical deformation and excitation becomes nonlinear when the excitation frequency approaches the fundamental natural frequencies. The large mechanical deformation near the fundamental natural frequencies influence the performance of the force sensor, represented by the distorted output charges as shown in Figure 5, and hence, should be avoided in the cutting force measurement. From Figure 4 and Figure 5, it can be seen that the force sensor can provide a linear operating range of approaching 10 kHz which is sufficient for providing the required 8.3 kHz frequency bandwidth.

Table 3: Parameters of A2 (304) Used in the Simulations [3].

	Thickness-Shear Mode Vibration due to F_X	Thickness-Shear Mode Vibration due to F_Y	Thickness-Stretch Mode Vibration due to F_Z
Mass density (kg/m^3)		$\rho_1 = 8030$	
Elastic constants ($10^{10}N/m^2$)	$c^1_{44} = 7.80$ $\hat{c}^1_{444} = 0$ $\hat{c}^1_{4444} = 11.32$	$c^1_{55} = 7.80$ $\hat{c}^1_{555} = 0$ $\hat{c}^1_{5555} = 11.32$	$c^1_{33} = 22.64$ $\hat{c}^1_{333} = 22.64$ $\hat{c}^1_{3333} = 11.32$

Note: Compact indices are used for elastic and piezoelectric stress constants in Tables 2 and 3.

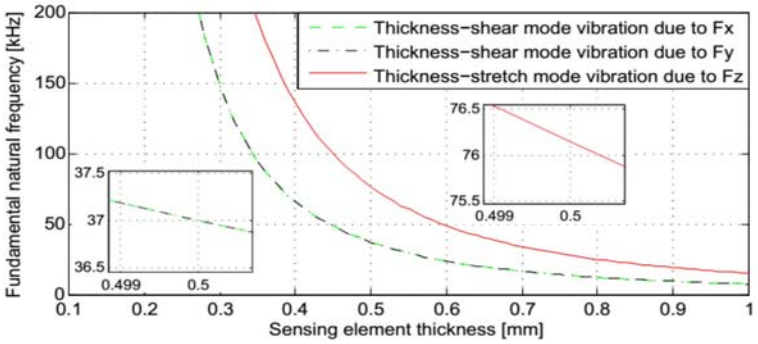

Figure 3: Fundamental Natural Frequencies W.R.T. Sensing Element Thickness.

5.3 Sensing resolution

Figure 6 presents the amplitude of the output charges with respect to input cutting forces for excitation frequency ranging up to 8.3 kHz, corresponding to the required frequency bandwidth. From Figure 6, it can be seen that the output charges possess a linear relationship with the input cutting forces within the frequency bandwidth. From the slope of the output charges, the sensitivity of the force sensor is defined as 325 pC/N while measuring F_X and F_Y, and 160 pC/N while measuring F_Z. This sensitivity indicates that for a unit output charge of 1pC, the force sensor can detect a 3 mN change in the input force signal while measuring F_X and F_Y, and 6 mN change in the input force signal while measuring F_Z. Namely, a sensing resolution of 3 mN is predicted when measuring F_X and F_Y and 6 mN, when measuring

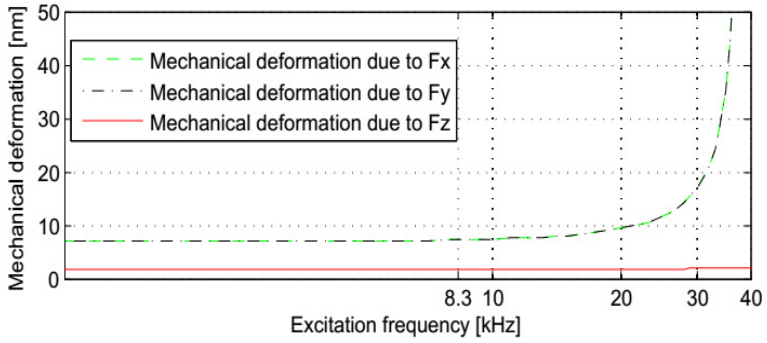

Figure 4: Mechanical Deformation W.R.T. Excitation Frequency Approaching Fundamental Natural Frequencies (with Force Amplitude of 15N).

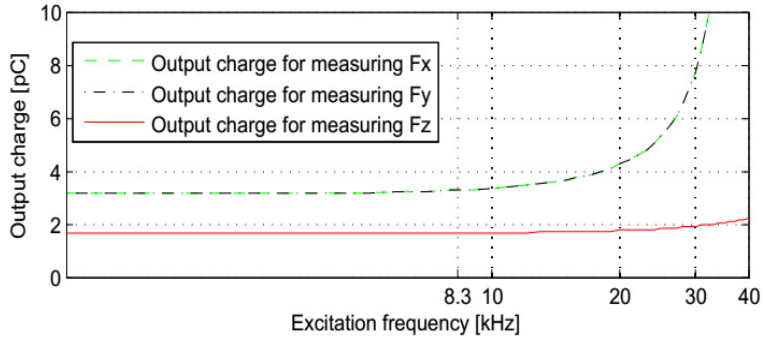

Figure 5: Output Charges W.R.T. Excitation Frequency Approaching Fundamental Natural Frequencies (with Force Amplitude of 10 mN).

F_Z.

6 Conclusion

This paper develops a mathematical model for use in the vibration analysis of a three-component piezoelectric force sensor which is designed for measuring the three-component cutting forces in meso-milling process. The vibration analysis model describes the nonlinear three dimensional vibrations in the sensory system due to the excitation of the oscillating input cutting forces. The analytical solutions of the vibration analysis model determine the sensor response, namely mechanical deformation and output charges, to the input cutting forces. The sensor response is then used to analyze

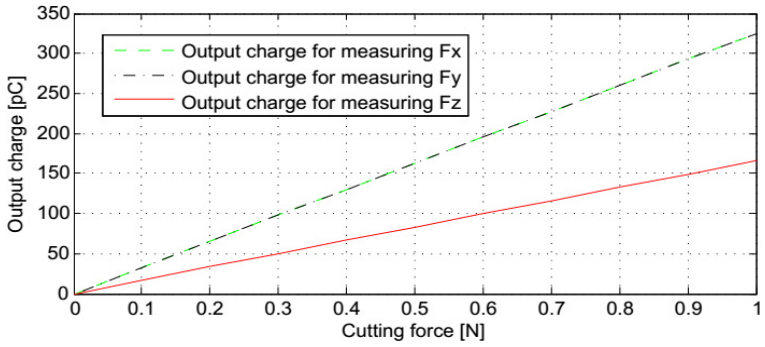

Figure 6: Output Charges W.R.T. Cutting Forces (with Oscillating Frequency of up to 8.3 kHz).

the sensor performance, including frequency bandwidth and sensing resolution, while measuring the three-component cutting forces in meso-milling process. Simulations with respect to the sensor response predict that the designed force sensor can provide required sensing resolution and frequency bandwidth needed for use in the proposed cutting force measurement.

Acknowledgements

This research is funded by the Natural Science and Engineering Research Council of Canada through the Canadian Network for Research and Innovation in Machining Technology (NSERC CANRIMT).

References

[1] A. Bedford, *Hamilton's Principle in Continuum Mechanics*, Pitman Advanced Publishing Program, Boston, 1985.

[2] J. Chae and S.S. Park, *High frequency bandwidth measurements of micro cutting forces*, Int. J. Mach.Tools Manufac. 47 (2007) 1433–1441.

[3] J.R. Davis, *Stainless Steels, Materials Park*, ASM International, Ohio, 1994.

[4] G. Gautschi, *Piezoelectric Sensorics: Force, Strain, Pressure, Acceleration and Acoustic Emission Sensors, Materials and Amplifiers*, Springer, Berlin, 2002.

[5] Y. Hu, H. Xue, J. Yang and Q. Jiang, *Nonlinear behavior of a piezoelectric power harvester near resonance*, IEEE Trans. Ultrason., Ferroelectr., Freq. Control **53** (2006) 1387–1391.

[6] J. Karki, *Signal Conditioning Piezoelectric Sensors*, Texas Instruments Incorporated, Dallas, 2000.

[7] T. Kenny, *Sensor Fundamentals in Sensor Technology Handbook*, Elsevier, Amsterdam, 2005.

[8] L.D. Landau and E.M. Lifshitz, *Theory of Elasticity*, Pergamon, New York, 1986.

[9] K.M. Liew, K. C. Hung and M. K. Lim, *Modeling three-dimensional vibration of elliptic bars*, J. Acoust. Soc. Am. **98** (1995) 1518–1526.

[10] J. Marsden and A. Weinstein, *Calculus I*, Springer, New York, 1985.

[11] J.N. Reddy, *Theory and Analysis of Elastic Plates and Shells*, CRC Press, Boca Raton, 2007.

[12] F. Shao, *Design of a three-component force sensor for meso-milling applications*, University of Toronto: Ph.D. Thesis, 2015.

[13] Sensor Tech., *Piezoelectric and dielectric constants for various piezoelectric materials*, Sensor Technology, Collingwood, Canada, 2011.

[14] J. Yang, Z. Chen, Y. Hu, S. Jiang and S. Guo, *Weakly nonlinear behavior of a plate thickness-mode piezoelectric transformer*, IEEE Trans. Ultrason., Ferroelectr., Freq. Control **54** (2007) 877–881.

[15] J. Yang, *An Introduction to the Theory of Piezoelectricity*, Springer, New York, 2005.

[16] J. Yang, *Piezoelectric transformer structural modeling–A review*, IEEE Trans. Ultrason., Ferroelectr., Freq. Control **54** (2007) 1154–1170.

[17] J. Yang, *The Mechanics of Piezoelectric Structures*, World Scientific, Singapore, 2006.

Apendix

Integration by parts is applied to the quadratic terms in (1) for the first variation. The procedures are illustrated herein for the quadratic term with

parameter ρ_0:

$$\begin{aligned}
\delta \int_{t_0}^{t_1} dt \int_0^{V_0} \frac{\rho_0}{2} \dot{y}_m^2 dV &= \rho_0 \int_0^{V_0} dV \int_{t_0}^{t_1} \delta \left(\frac{1}{2} \dot{y}_m^2 \right) dt \\
&= \rho_0 \int_0^{V_0} dV \int_{t_0}^{t_1} \dot{y}_m \delta \dot{y}_m dt \\
&= \rho_0 \int_0^{V_0} dV \int_{t_0}^{t_1} \delta \dot{y}_m dy_m \\
&= \rho_0 \int_0^{V_0} dV \int_{t_0}^{t_1} \dot{y}_m d\delta y_m \\
&= \rho_0 \int_0^{V_0} dV \left\{ \left(\delta y_m \dot{y}_m \right) |_{t_0}^{t_1} - \int_{t_0}^{t_1} \delta y_m d\dot{y}_m \right\} \\
&= \rho_0 \int_0^{V_0} dV \left\{ 0 - \int_{t_0}^{t_1} \delta y_m \ddot{y}_m dt \right\} \\
&= \int_{t_0}^{t_1} dt \int_0^{V_0} \left\{ -\rho_0 \ddot{y}_m \delta y_m \right\} dV
\end{aligned}$$

The method and procedures also apply to the quadratic term with parameter ρ_1.